Chapter 5

NUCLEAR RADIO POLARIZATION

AND MISALIGNMENT IN RADIO STRUCTURES

Polarized radiation from regions around active galactic nuclei is a powerful probe of the physical conditions prevailing in those regions in several different ways. Its behaviour is an important diagnostic of the emission mechanism and/or the (polarizing) propagation effects along the line of sight. More fundamentally, the very existence of polarized radiation implies the absence of complete symmetry or complete disorder, either in the structuring of the emitting material or in the polarizing agents along the line of sight.

Observations at high angular resolution have shown that the radio emission from the nuclear components of radio quasars and galaxies *is* polarized, though at very low levels as compared to the degree of polarization seen in the large-scale jets and lobes. In this chapter, polarization data have been used to infer the geometry of the central regions of radio-powerful active galactic nuclei (RPAGN), and to examine how this geometry relates to the radio structure on the large scale. The results for radio quasars are discussed in the context of the relativistic beaming hypothesis. The case of radio galaxies has also been considered.

Similar investigations with *optical* polarization have been done before. It has been found that in the 'LPQs' (the QSOs that show 'low'—i.e., $\lesssim 3$ percent—optical polarization) that have double radio lobes, the position angle (PA) of the polarization was roughly aligned with the radio structure (Moore & Stockman, 1984, and references therein). This result implies that the PA of the optical polarization must be relatively constant over the lifetime of the source, i.e., over scales of ~ 10^7 years.

5.1 Misalignments in radio structure

The study of the structural alignment between the nuclear jets and the larger scale extensions in RPAGN is important because it yields estimates of the time scales over which the ejection axis of the effluent remains stable, and hence provides constraints on models for jet formation. Besides, as has been elaborated in the introductory chapter, the question of misalignment of radio structures of quasars is directly relevant to the unified scheme. At inclination angles of sources that are close to the line of sight, any intrinsic misalignments are amplified for most lines of sight; and since in the unified scheme, core-dominated quasars (CDQs) are believed to be at small angles to the line of sight, it follows that there should be larger misalignments between nuclear and large scale structure in them as compared to lobe-dominated quasars (LDQs).

5.1.1 Insights from Very Long Baseline Interferometry

The study of radio sources at angular resolutions of the order of milliarcseconds has been made possible by the introduction of Very Long Baseline Interferometry (VLBI). One of the most important conclusions reached by the early VLBI investigations of radio-powerful active galactic nuclei was the following: objects with 'symmetric' type of (large scale) radio structure (*i.e.*, the 'classical double' sources with steep overall radio spectrum and projected linear sizes $\gtrsim$ 100 kpc) showed a high degree of alignment between the most compact and the most extended features. On the other hand, those with 'core' type of structure (*i.e.*, sources with flat overall radio spectrum, smaller projected linear sizes of $\lesssim$ 100 kpc, and the radio component coincident with the QSO dominating the emission) showed a range of orientations of their structures on different scales (Readhead *et al.*, 1978). In the sample of Readhead *et al.* (1978), there were five sources of the 'symmetric' type (all nearby radio galaxies, of redshifts < 0.1) and four of the 'core' type (all quasars, of larger redshifts). From similar VLBI data for three radio quasars with one-sided radio structure, Davis *et al.* (1978) concluded that the nuclear elongations were typically misaligned by $\sim 20°$ with the axis of the overall radio structure. This finding is similar to that of Readhead *et al.* (1978) for the 'core'-type objects.

Readhead *et al.* (1983) enlarged the older sample to 18 objects and confirmed the earlier conclusions. Their new sample had eight objects of the 'symmetric' type (of which seven are radio galaxies of redshift < 0.1 and one is a quasar), and ten of the 'core' type (of which eight are quasars and two are nearby BL Lacertids). They concluded that the distribution of the observed angles of misalignment for the sample was consistent with the relativistic beaming model, with an assumed intrinsic bend angle of $\sim 10°$ and Lorentz factor γ of 10. It must, however, be noted that in the context of the unified scheme, the comparison of misalignments should really be made specifically between radio *quasars* of the 'symmetric' and 'core' types. Also, the above findings need to be verified for a larger sample of objects.

VLBI observations entail international collaborative effort; moreover, due to limitations of sensitivity, only objects with the brightest nuclear components (which usually turn out to be those with relatively more prominent nuclei) can be observed. As a result, large collections of radio structures on angular scales of milliarcseconds are not easy to come by, and particularly not for objects with a wide range in core dominance.

5.2 An alternative approach

An alternative route is adopted here to study the question of misalignment. The orientation of the nuclear jet is inferred from the PA of the polarized emission from the nuclear component, as measured at $\lambda 6$ cm with angular resolutions of $\lesssim 1$ arcsec. (Such observations made with the VLA are available for several radio quasars). This approach entails the following assumptions:

(a) that the polarized emission observed from the central component using angular resolutions of $\lesssim 1$ arcsec is dominated by radiation from the optically thin (unresolved) nuclear jet (cf. Fig. 5.1);

(b) that Faraday rotation at wavelengths as short as $\lambda 6$ cm is ignorable, so that the observed orientation of the E−vector of the radiation is close to the intrinsic one;

(c) that the nuclear jet is optically thin at these frequencies, so that the orientation of the observed polarized (synchrotron) radiation is perpendicular to the magnetic field in the jet; and

(d) that the direction of the magnetic field bears a fixed relation (specifically,

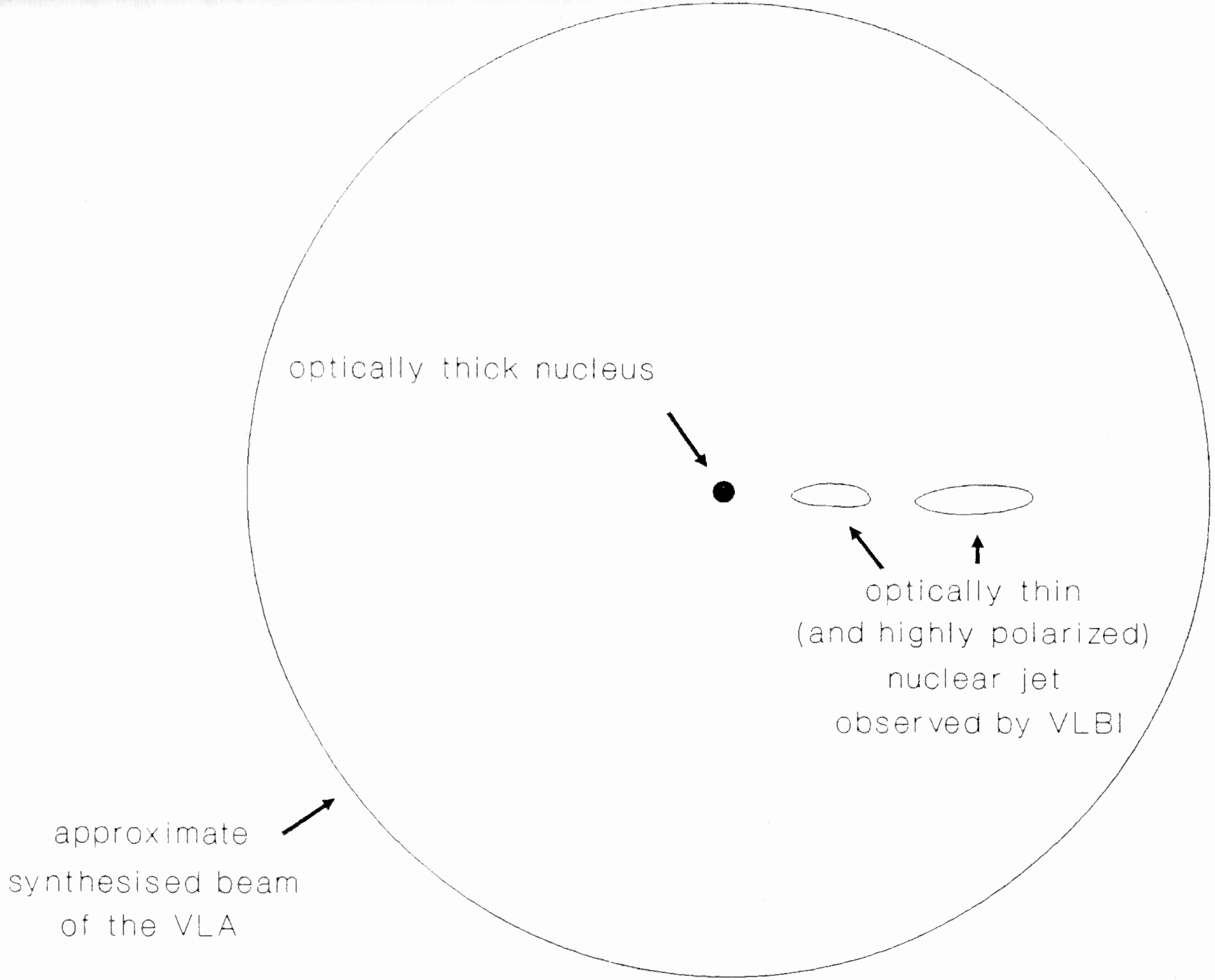

Figure 5.1. Illustration of assumption (a)

perpendicular) to the axis of the nuclear jet.

To ensure that (a) holds, the sample has been constituted from objects for which high angular resolution VLA observations are available, so that the observed polarized emission from the nuclear component is not contaminated by larger scale structure.

To ensure that (b) holds, it is important to avoid those directions in the sky where effects of propagation through our Galaxy are known to rotate the plane of polarization significantly. Simard-Normandin & Kronberg (1980) have calculated rotation measures (RMs) from linear polarization measurements made at several wavelengths for 552 extragalactic objects spanning the whole sky. The results show that directions through the Galactic plane (up to latitudes of about 15°) show large positive RM. Also, there appears to be a region below the plane around longitude of about 90° that shows a large negative RM. Candidate objects for the present study that occur in these regions have been excluded from the analysis. Fig. 5.2 shows a map of the sky with equatorial and Galactic coordinates marked. The areas of sky excluded from the present analysis are shown hatched.

Large scale jets observed in quasars and radio galaxies are known to be generally optically thin, and it is expected that the nuclear jets are qualitatively similar in this respect (premise (c)). Multifrequency VLBI maps in a few cases have shown that this is indeed so (e.g., Eckart *et al.*, 1987).

Premise (d) obtains by extrapolating from observations of large scale jets in radio quasars (Owen & Puschell, 1984), and from the following finding of Davis *et al.* (1978) for nuclear jets. For the three radio quasars in their investigation, the

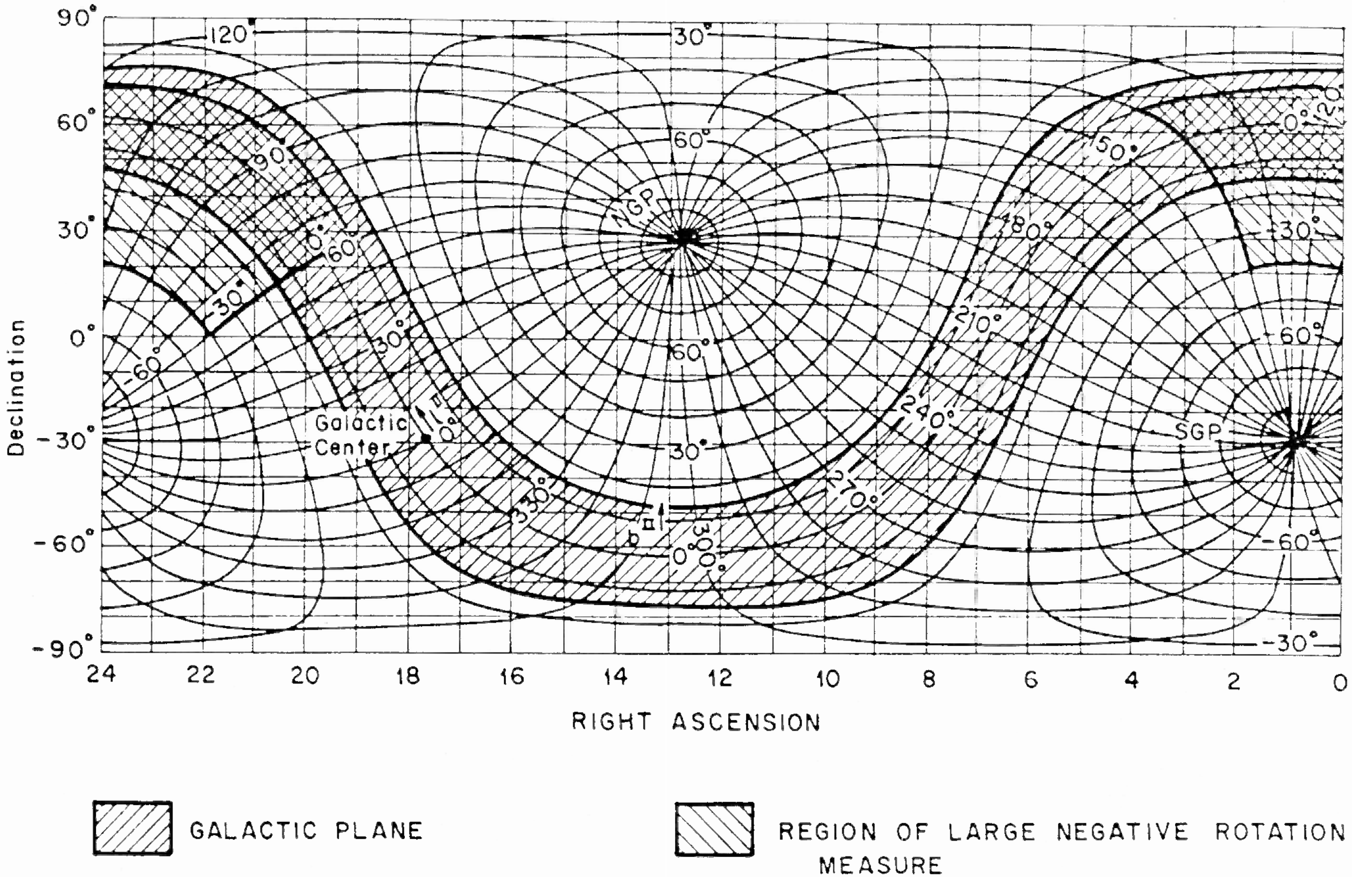

Fig. 5.2. Excluded regions of the sky.

magnetic field directions in the subcomponents (as derived from interferometric polarimetry) appeared to coincide with the structural elongations of the component. This assumption has subsequently been vindicated *for the CDQs* by several later workers (e.g., Rusk & Seaquist (1985); Jones *et al.* 1985; O'dea *et al.*, 1988; Wrobel *et al.*, 1988).

If all the above assumptions are valid, then the direction of the nuclear jet is, to a good approximation, perpendicular to the orientation of the observed polarization at $\lambda 6$ cm.

5.3 The sample and the selection criteria

The sample has been compiled by choosing from among the radio images of quasars that were presented in Chapter 3 (which have polarization data measured with the VLA) and from VLA polarization data for quasars in the literature. The latter are listed in Table 5.1.

Table 5.1 Sources of high-resolution polarimetry.

Chapter 3, this thesis	Rudnick et al. (1985)
Feigelson et al.(1984)	Rudnick et al. (1986)
Gower & Hutchings (1982)	Rudnick & Jones (1982)
Harris et al. (1983)	Rudnick & Jones (1983)
O'dea et al. (1988)	Saikia et al. (1983)
Owen & Puschell (1984)	Saikia et al. (1985)
Padrielli et al. (1988b)	Stocke et al. (1985)
Perley et al. (1980)	Swarup et al. (1982)
Perley et al. (1982)	Swarup et al. (1984)
Perley (1982)	Swarup et al. (1986)
Potash & Wardle (1980)	Wardle & Potash (1982)

The selection criteria adopted are the following:

(i) The VLA polarization data are required to be of good signal-to-noise and thus usable to estimate the orientation of the polarization. Data with estimated error in the polarization PA of more than 20° have been excluded.

(ii) Sources in the Galactic plane region (latitudes $|b| < 15°$), or lying in the Galactic region $60° < l < 140°$ and $-40° < b < 10°$, have to be excluded. The latter is a region of large negative RM (Simard-Normandin & Kronberg 1980). The RMs for $|b| \gtrsim 15°$ are usually $\lesssim 30$ rad m^{-2}.

(iii) Two-sided quasars whose large scale structure is highly bent are excluded. In these objects, a comparison of the PA of the core polarization with the line joining the outer lobes is not very meaningful. Only those sources for which the supplement of the angle formed at the nucleus by the outer lobes/hot spots is $\lesssim 25°$ are included. This 'misalignment cutoff' resulted in the exclusion of 12 objects.

The final list consists of 133 objects. Here, no attempt has been made to distinguish between quasars and BL Lacertids.

5.4 The derived parameters

The objects in the sample and their properties are listed in Table 5.2 which is arranged as follows:

Column 1: the name of the quasar (followed by an asterisk if the polarization data are from B or C-array of the VLA; for the rest, A-array data have been used).

Column 2: the radio structure-type, *viz.*, 'two-sided' or 'one-sided'.

Column 3: the redshift.

Column 4: the projected linear size (q_0 = 0.5, H_0 = 50 km s^{-1} Mpc^{-1}).

Column 5: PA of the core polarization E–vector at λ6 cm.

Column 6: PA of the radio structure axis.

Column 7: the angle ϕ, the difference between the two PAs above (cf. Fig. 5.3). (For the 'two-sided' quasars the radio axis is defined by the hot spots at the outer extremities of the source, while for the 'one-sided' objects, it is defined by the core and the single outer component.)

Column 8: the prominence of the radio nuclear component in the quasar rest frame, R_{emit} (emitted frequency of 8 GHz; cf. this thesis, Section 4.4.1). The few quasars that have no measured redshift have been assumed to be at a redshift of 1.

Column 9: reference codes for the sources of the polarization data and extended structure (from which the PA of the radio axis has been derived). The references are listed in **Table 5.3**.

The structure-type for some of the objects in the table has been noted as 'one-sided?', and these objects have no listed projected linear sizes. All these objects are from Perley (1982). Their structure-type and angular extents are uncertain because, in the course of the deconvolution of the images, fairly small search/CLEAN windows were used, and so one or more secondary components of a quasar may have been missed. For this reason, as noted by Perley himself, some sources listed as having only a single secondary component may actually have more components

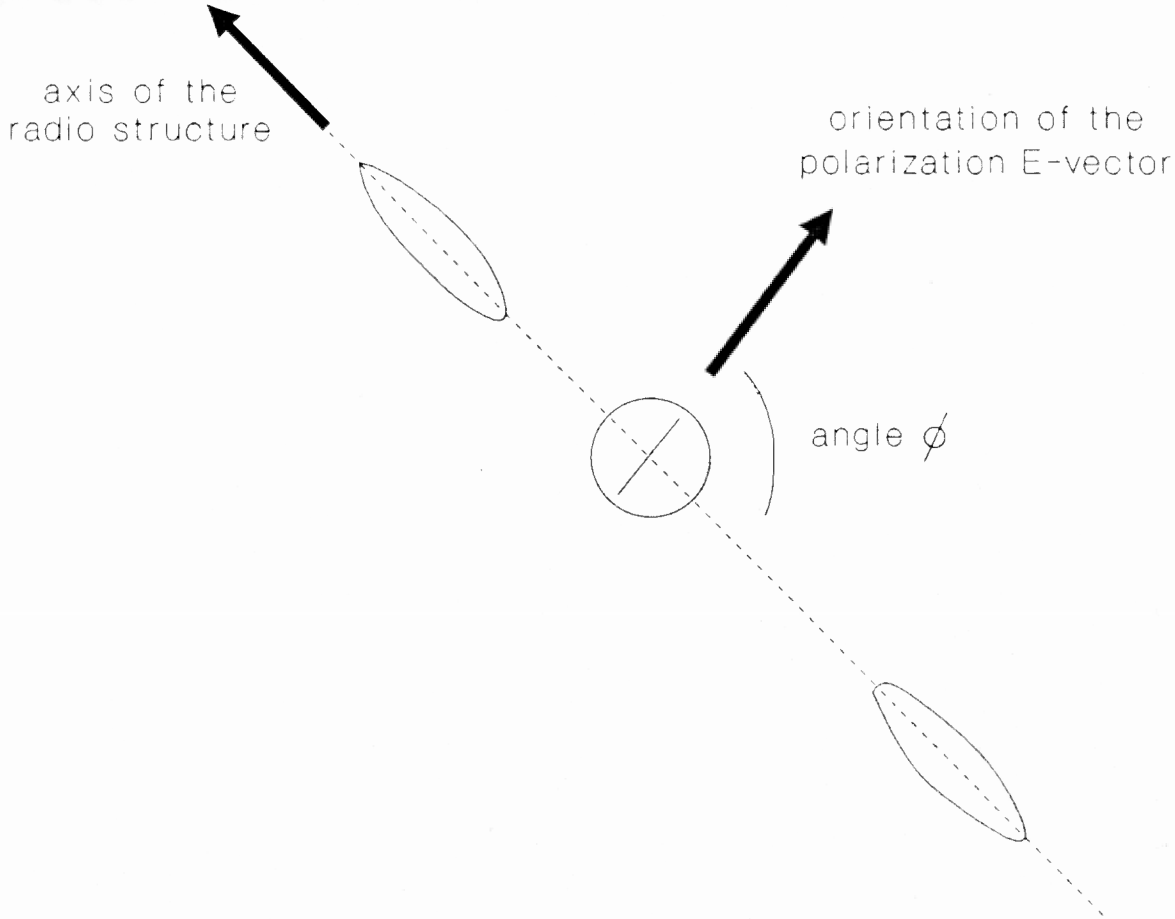

Figure 5.3 The parameter ϕ

Table 5.2 The sample of quasars

Source	Structure type	Redshift	Projected linear size (kpc)	Core Polarization PA (°)	Structure PA (°)	ϕ (°)	R	References
0048-097	one-sided?			55	9	46	1.02	P82
0106+013	one-sided	2.107	32.4	151	5	34	4.30	P82; BP
0112-017	one-sided	0.284	37.8	60	130	70	57.57	P82; BP
0113-118	one-sided	0.672	39.4	60	162	78	2.21	P82; BP
0115+027	two-sided	0.672	104.8	163	73	90	0.32	present
0135-247	one-sided?	0.831		170	92	78	0.91	P82
0202-172	one-sided	1.740	111.7	116	55	61	12.94	P82; BP
0216+011	one-sided?			36	145	71	12.85	P82
0221+067	one-sided		130.3	36	101	65	3.55	P82; BP
0237+040	one-sided?	0.978		43	145	4	4.97	P82
0239+108	one-sided?			45	40	5	63.75	P82
0319+121	one-sided		106.4	67	162	85	96.75	P82; BP
0333+321	two-sided	1.263	68.9	57	146	89	50.19	P82; OB; SdB
0336-019	one-sided	0.852	43.3	155	165	10	399.52	P82; BP
0400-319	one-sided?			163	50	67	2.56	P82
0402-362	one-sided?	1.417		67	170	77	10.00	P82
0420-014	two-sided	0.915	347.0	64	10	54	206.25	P82; A
0426-380	one-sided?			110	156	46	57.84	P82
0438-436	one-sided?	2.852		19	15	4	22.58	P82
0440-003	one-sided	0.844	8.3	23	90	67	0.61	P82; BP
0451-282	one-sided?	2.559		82	170	88	1.27	P82
0511-220	one-sided?			149	120	29	2.36	P82
0514-161	one-sided?	1.278		1	55	54	9.39	P82
0528-250	one-sided?	2.765		104	80	24	2.22	P82
0539-057	one-sided?			95	50	45	3.31	P82
0609+607	one-sided?			100	90	10	90.14	P82
0707+476	two-sided	1.310	73.2	115	90	25	1.47	P82; BP
0716+714	two-sided		81.7	3	119	64	0.81	P82; PFJ80
0723+679	two-sided	0.846	128.6	172	82	90	0.40	OP
0735+178	one-sided		17.0	80	170	90	37.24	P82; BP
0742+376	one-sided		530.4	175	132	43	0.40	present
0745+241	two-sided		127.7	27	65	38	6.71	P82
0759+183	one-sided?			65	95	30	10.49	P82
0812+367	two-sided	1.025	152.8	65	156	89	3.19	P82; PFJ82
0820+560	one-sided?	1.417		7	130	57	43.93	P82
0821+447	two-sided	0.904	220.5	52	134	82	0.07	OP

Table 5.2 (contd.)

Source	Structure type	Redshift	Projected linear size (kpc)	Core Polarization PA (°)	Structure PA (°)	ϕ (°)	R	References
0821+621	two-sided	0.542	337.7	133	52	81	6.35	OP
0827+243	one-sided?	0.939		37	20	17	1.40	P82
0833+585	one-sided	2.101	94.0	170	155	15	3.50	P82; BP
0836+195	two-sided	1.691	263.2	109	14	85	0.47	present
0836+710	one-sided	2.160	16.1	102	24	78	16.52	P82; PFJ82; OB
0850+581	two-sided	1.322	128.5	110	145	35	1.69	RJ82; HUO
0851+202	one-sided	0.306	155.0	87	115	28	9.91	P82; dBS
0859+470	one-sided	1.462	24.8	68	150	82	14.76	P82; PFJ80; BP
0859-140	two-sided	1.327	103.3	75	162	87	49.05	OB; BP
0906+430	two-sided	0.670	23.6	74	60	14	1.34	RJ82; WMA
0919+218	two-sided	1.421	96.1	129	46	83	0.07	present
0923+392	two-sided	0.699	30.3	176	73	77	6.35	P82; B82
0945+408	one-sided	1.252	35.3	12	35	23	2.15	P82; PFJ82; BP
0954+658	one-sided	0.368	23.4	161	25	44	1.09	P82; BP
0955+476	two-sided	1.873	165.9	58	120	62	166.67	P82
1004-018	one-sided?	1.212		29	130	79	4.70	P82
1007+417	two-sided	0.611	245.0	104	7	83	0.27	present; OP
1012+232	two-sided	0.565	134.2	179	176	3	7.53	present
1020-103	one-sided?	0.197		120	150	30	14.08	P82
1021-006	one-sided?	2.547		167	10	23	13.64	P82
1028+313	one-sided	0.177	32.5	60	176	64	2.33	FIK
1032-199	one-sided	2.198	21.6	92	145	53	2.24	P82; BP
1040+123	two-sided	1.029	63.2	24	92	68	3.01	present
1055+018	two-sided	0.888	251.5	101	180	79	35.75	present;P82;OB; BP
1055+201	two-sided	1.110	182.0	93	11164.5	71.5	2.26	present
1116+128	one-sided	2.118	24.3	120	135	15	5.97	P82; OB; BP
1132+303	two-sided	0.614	118.9	88	143	55	0.27	present
1136-135	two-sided	0.554	117.7	13	129	64	0.28	present
1147+245	two-sided		183.4	18	170	28	2.27	P82; A
1148-001	one-sided	1.982	38.6	143	30	67	14.72	P82; BP
1150+497	two-sided	0.334	90.1	123	8	65	0.85	P82; OP
1150+812	one-sided	1.250	43.1	102	80	22	43.67	P82; BP
1156+295	two-sided	0.729	31.0	120	0	60	4.78	P82; A
1213+350	two-sided	0.851	116.5	117	25	88	43.30	P82
1221+186	two-sided	1.401	202.7	44	124	80	0.24	SSH
1221+809	two-sided		26.4	147	17	50	5.20	P82; PFJ80

Table 5.2 (contd.)

Source	Structure type	Redshift	Projected linear size (kpc)	Core Polarization PA (°)	Structure PA (°)	ϕ (°)	R	References
1226+023	one-sided	0.158	74.6	155	42	67	3.57	P82; P81
1236+077	one-sided?			128	65	63	10.30	P82
1237-101	one-sided	0.753	138.0	47	30	17	2.32	P82; BP
1243-072	one-sided	1.286	25.8	20	80	60	2.99	P82; BP
1252+119	one-sided	0.871	16.7	153	110	43	2.79	P82; BP
1317+520	two-sided	1.060	250.8	33	130	83	0.75	OP; HUO
1320+299	one-sided		32.2	132	101	31	3.44	present
1347+539	one-sided	0.976	45.0	13	138	55	4.04	present; P82; OP
1354+195	two-sided	0.720	350.8	67	167	80	4.85	present; P82; RR
1354-152	one-sided	1.890	23.2	130	90	40	9.40	P82; BP
1415+463	one-sided	1.552	112.5	172	83	89	4.45	present; OP
1418+546	one-sided		290.0	175	83	88	158.78	P82; A
1430-178	one-sided?	2.331		5	90	85	1.03	P82
1433+177	two-sided	1.203	86.1	64	172	72	0.46	present
1434+235	one-sided?			92	20	72	131.02	P82
1435+315	two-sided	1.366	103.2	156	137	19	2.40	SSH; RPdR
1435+638	one-sided	2.060	122.1	156	50	74	1.15	P82; BP
1451-375	two-sided	0.314	169.4	150	60	90	4.33	P82
1502+106	one-sided	1.839	58.3	178	160	18	1.46	P82; BP
1509+158	two-sided	0.828	68.7	147	68	79	0.16	present
1510-089	one-sided	0.361	54.9	79	160	81	15.52	P82; OP; BP
1514-241	one-sided	0.049	30.1	50	98	48	485.75	P82; A
1524+101	two-sided	1.358	92.9	128	46	82	0.75	FIK
1551+130	one-sided?	2.21		95	75	20	1.16	P82
1555+332	two-sided	0.942	301.8	10	95	85	1.50	FIK
1616+063	one-sided?	2.086		51	45	6	8.22	P82
1636+473	one-sided	0.740	161.7	58	25	33	3.35	present; P82
1637+574	one-sided	0.745	32.4	108	98	10	36.49	present; P82
1638+398	one-sided	1.660	21.1	176	140	36	1.17	P82; BP
1642+690	two-sided	0.751	81.1	144	2	38	9.33	P82; BO81
1656+053	one-sided	0.887	18.4	176	110	66	2.14	P82; BP
1716+686	one-sided?	0.777		91	130	39	4.64	P82
1717+178	one-sided		80.9	18	6	12	9.56	P82; AU
1725+044	one-sided	0.296	27.8	15	105	90	3.75	P82; BP
1725+123	one-sided?			94	135	41	1.39	P82
1729+501	one-sided	1.107	175.1	50	11136.5	86.5	0.07	Present; OP

Table 5.2 The sample of quasars

Source	Structure type	Redshift	Projected linear size (kpc)	Core Polarization PA (°)	Structure PA (°)	Ø (°)	R	References
0048-097	one-sided?			55	9	46	1.02	P82
0106+013	one-sided	2.107	32.4	151	5	34	4.30	P82; BP
0112-017	one-sided	0.284	37.8	60	130	70	57.57	P82; BP
0113-118	one-sided	0.672	39.4	60	162	78	2.21	P82; BP
0115+027*	two-sided	0.672	104.8	163	73	90	0.32	present
0135-247	one-sided?	0.831		170	92	78	0.91	P82
0202-172	one-sided	1.740	111.7	116	55	61	12.94	P82; BP
0216+011	one-sided?			36	145	71	12.85	P82
0221+067	one-sided		130.3	36	101	65	3.55	P82; BP
0237+040	one-sided?	0.978		43	145	4	4.97	P82
0239+108	one-sided?			45	40	5	63.75	P82
0319+121	one-sided		106.4	67	162	85	96.75	P82; BP
0333+321	two-sided	1.263	68.9	57	146	89	50.19	P82; OB; SdB
0336-019	one-sided	0.852	43.3	155	165	10	399.52	P82; BP
0400-319	one-sided?			163	50	67	2.56	P82
0402-362	one-sided?	1.417		67	170	77	10.00	P82
0420-014	two-sided	0.915	347.0	64	10	54	206.25	P82; A
0426-380	one-sided?			110	156	46	57.84	P82
0438-436	one-sided?	2.852		19	15	4	22.58	P82
0440-003	one-sided	0.844	8.3	23	90	67	0.61	P82; BP
0451-282	one-sided?	2.559		82	170	88	1.27	P82
0511-220	one-sided?			149	120	29	2.36	P82
0514-161	one-sided?	1.278		1	55	54	9.39	P82
0528-250	one-sided?	2.765		104	80	24	2.22	P82
0539-057	one-sided?			95	50	45	3.31	P82
0609+607	one-sided?			100	90	10	90.14	P82
0707+476	two-sided	1.310	73.2	115	90	25	1.47	P82; BP
0716+714	two-sided		81.7	3	119	64	0.81	P82; PFJ80
0723+679	two-sided	0.846	128.6	172	82	90	0.40	OP
0735+178	one-sided		17.0	80	170	90	37.24	P82; BP
0742+376*	one-sided		530.4	175	132	43	0.40	present
0745+241	two-sided		127.7	27	65	38	6.71	P82
0759+183	one-sided?			65	95	30	10.49	P82
0812+367	two-sided	1.025	152.8	65	156	89	3.19	P82; PFJ82
0820+560	one-sided?	1.417		7	130	57	43.93	P82
0821+447	two-sided	0.904	220.5	52	134	82	0.07	OP

Table 5.2 (contd.)

Source	Structure type	Redshift	Projected linear size (kpc)	Core Polarization PA (°)	Structure PA (°)	Ø (°)	R	References
0821+621	two-sided	0.542	337.7	133	52	81	6.35	OP
0827+243	one-sided?	0.939		37	20	17	1.40	P82
0833+585	one-sided	2.101	94.0	170	155	15	3.50	P82; BP
0836+195*	two-sided	1.691	263.2	109	14	85	0.47	present
0836+710	one-sided	2.160	16.1	102	24	78	16.52	P82; PFJ82; OB
0850+581*	two-sided	1.322	128.5	110	145	35	1.69	RJ82; HUO
0851+202	one-sided	0.306	155.0	87	115	28	9.91	P82; dBS
0859+470	one-sided	1.462	24.8	68	150	82	14.76	P82; PFJ80; BP
0859-140	two-sided	1.327	103.3	75	162	87	49.05	OB; BP
0906+430*	two-sided	0.670	23.6	74	60	14	1.34	RJ82; WMA
0919+218	two-sided	1.421	96.1	129	46	83	0.07	present
0923+392	two-sided	0.699	30.3	176	73	77	6.35	P82; B82
0945+408	one-sided	1.252	35.3	12	35	23	2.15	P82; PFJ82; BP
0954+658	one-sided	0.368	23.4	161	25	44	1.09	P82; BP
0955+476	two-sided	1.873	165.9	58	120	62	166.67	P82
1004-018	one-sided?	1.212		29	130	79	4.70	P82
1007+417	two-sided	0.611	245.0	104	7	83	0.27	present; OP
1012+232	two-sided	0.565	134.2	179	176	3	7.53	present
1020-103	one-sided?	0.197		120	150	30	14.08	P82
1021-006	one-sided?	2.547		167	10	23	13.64	P82
1028+313*	one-sided	0.177	32.5	60	176	64	2.33	FIK
1032-199	one-sided	2.198	21.6	92	145	53	2.24	P82; BP
1040+123	two-sided	1.029	63.2	24	92	68	3.01	present
1055+018	two-sided	0.888	251.5	101	180	79	35.75	present; P82; OB; BP
1055+201	two-sided	1.110	182.0	93	165	72	2.26	present
1116+128	one-sided	2.118	24.3	120	135	15	5.97	P82; OB; BP
1132+303	two-sided	0.614	118.9	88	143	55	0.27	present
1136-135	two-sided	0.554	117.7	13	129	64	0.28	present
1147+245	two-sided		183.4	18	170	28	2.27	P82; A
1148-001	one-sided	1.982	38.6	143	30	67	14.72	P82; BP
1150+497	two-sided	0.334	90.1	123	8	65	0.85	P82; OP
1150+812	one-sided	1.250	43.1	102	80	22	43.67	P82; BP
1156+295	two-sided	0.729	31.0	120	0	60	4.78	P82; A
1213+350	two-sided	0.851	116.5	117	25	88	43.30	P82
1221+186	two-sided	1.401	202.7	44	124	80	0.24	SSH
1221+809	two-sided		26.4	147	17	50	5.20	P82; PFJ80

Table 5.2 (contd.)

Source	Structure type	Redshift	Projected linear size (kpc)	Core Polarization PA (°)	Structure PA (°)	Ø (°)	R	References
1226+023	one-sided	0.158	74.6	155	42	67	3.57	P82; P81
1236+077	one-sided?			128	65	63	10.30	P82
1237-101	one-sided	0.753	138.0	47	30	17	2.32	P82; BP
1243-072	one-sided	1.286	25.8	20	80	60	2.99	P82; BP
1252+119	one-sided	0.871	16.7	153	110	43	2.79	P82; BP
1317+520	two-sided	1.060	250.8	33	130	83	0.75	OP; HUO
1320+299	one-sided		32.2	132	101	31	3.44	present
1347+539	one-sided	0.976	45.0	13	138	55	4.04	present; P82; OP
1354+195	two-sided	0.720	350.8	67	167	80	4.85	present; P82; RR
1354-152	one-sided	1.890	23.2	130	90	40	9.40	P82; BP
1415+463	one-sided	1.552	112.5	172	83	89	4.45	present; OP
1418+546	one-sided		290.0	175	83	88	158.78	P82; A
1430-178	one-sided?	2.331		5	90	85	1.03	P82
1433+177*	two-sided	1.203	86.1	64	172	72	0.46	present
1434+235	one-sided?			92	20	72	131.02	P82
1435+315	two-sided	1.366	103.2	156	137	19	2.40	SSH; RPdR
1435+638	one-sided	2.060	122.1	156	50	74	1.15	P82; BP
1451-375	two-sided	0.314	169.4	150	60	90	4.33	P82
1502+106	one-sided	1.839	58.3	178	160	18	1.46	P82; BP
1509+158	two-sided	0.828	68.7	147	68	79	0.16	present
1510-089	one-sided	0.361	54.9	79	160	81	15.52	P82; OP; BP
1514-241	one-sided	0.049	30.1	50	98	48	485.75	P82; A
1524+101*	two-sided	1.358	92.9	128	46	82	0.75	FIK
1551+130	one-sided?	2.21		95	75	20	1.16	P82
1555+332*	two-sided	0.942	301.8	10	95	85	1.50	FIK
1616+063	one-sided?	2.086		51	45	6	8.22	P82
1636+473	one-sided	0.740	161.7	58	25	33	3.35	present; P82
1637+574	one-sided	0.745	32.4	108	98	10	36.49	present; P82
1638+398	one-sided	1.660	21.1	176	140	36	1.17	P82; BP
1642+690	two-sided	0.751	81.1	144	2	38	9.33	P82; BO81
1656+053	one-sided	0.887	18.4	176	110	66	2.14	P82; BP
1716+686	one-sided?	0.777		91	130	39	4.64	P82
1717+178	one-sided		80.9	18	6	12	9.56	P82; AU
1725+044	one-sided	0.296	27.8	15	105	90	3.75	P82; BP
1725+123	one-sided?			94	135	41	1.39	P82
1729+501	one-sided	1.107	175.1	50	137	87	0.07	present; OP

Table 5.2 (contd.)

Source	Structure type	Redshift	Projected linear size (kpc)	Core Polarization PA (°)	Structure PA (°)	Ø (°)	R	References
1739+522	one-sided	1.375	30.1	67	80	13	15.30	P82; BP
1741+279	two-sided	0.372	62.6	71	171	80	0.59	present
1743+173	one-sided?	1.702		68	35	33	10.00	P82
1751+441	two-sided	0.871	117.0	10	77	67	4.48	P82; PFJ82; BP
1800+440	two-sided	0.660	79.6	138	68	70	1.83	P82; B82; BP
1803+784	one-sided		385.2	75	14	62	3.23	P82; A
1807+279	two-sided	1.760	83.9	162	45	63	0.46	P82
1823+568	one-sided	0.664	117.8	31	97	66	7.27	P82; OB
1842+681	one-sided	0.475	27.8	37	144	73	26.16	present
1849+670	one-sided?			47	30	17	16.67	P82
1857+566	two-sided	1.595	254.9	29	135	74	0.03	S83; OP
1933-400	one-sided?			64	140	76	0.68	P82
2007+777	one-sided		223.0	68	80	12	27.11	P82; BP
2010+723	one-sided?			149	103	46	14.45	P82
2044-168	one-sided?	1.937		56	145	89	1.51	P82
2058-297	one-sided?			80	34	46	6.74	P82
2131-021	one-sided?	0.557		168	135	33	265.51	P82
2155-152	two-sided		46.8	31	0	31	2.34	P82
2210-257	one-sided?	1.833		25	10	15	59.51	P82
2216-038	one-sided	0.901	67.2	85	140	55	5.71	P82; BP
2243-123	one-sided	0.630	30.1	178	40	42	53.84	P82; BP
2251+134	two-sided	0.673	52.0	108	40	68	0.99	present; P82
2308+098	two-sided	0.432	544.5	60	143	83	0.44	S86
2318+049	one-sided	0.622	65.4	63	135	72	3.12	P82; BP
2329-162	one-sided	1.155	16.3	179	50	51	2.14	P82; BP

Table 5.3 List of References

A	Antonucci et al. (1986)	present	Chapter 3, this thesis
AU	Antonucci & Ulvestad (1985)	RJ82	Rudnick & Jones (1982)
B82a	Browne et al. (1982a)	R85	Rudnick et al. (1985)
B82b	Browne et al. (1982b)	RPdR	Rogora et al. (1986))
B87	Browne (1987)	RR	Rusk & Rusk (1986)
BP	Browne & Perley (1986)	S83	Saikia et al. (1983)
dBS	de Bruyn & Schilizzi (1986)	SSK	Saikia et al. (1985)
FIK	Feigelson et al.(1984)	SSS	Saikia et al. (1984)
HUO	Hintzen et al. (1983)	SSH	Swarup et al.(1984)
OBC	O'dea et al. (1988)	S86	Swarup et al. (1986)
OP	Owen & Puschell (1984)	SdB	Schilizzi & de Bruyn (1983)
P82	Perley (1982)	WMA	Wardle et al. (1984)
PFJ80	Perley et al. (1980)	W82	Wilkinson (1982)
PFJ82	Perley et al. (1982)		

even with his dynamic ranges and may not be 'one-sided'. For example, Perley (1982) lists only an intense feature of the jet in the two-sided quasar 0742+318. Similarly, for 1354+195, another two-sided source, only one of the outer components is listed. Quasars that are noted as having only one secondary component in Perley (1982) and with no confirmatory image elsewhere in the literature, have therefore been marked as of uncertain structure-type in Table 5.2, and no projected linear size has been listed for them.

5.5 The results

The distribution of ϕ for the quasars in the sample is plotted in Fig. 5.4. It shows, on the one hand, a large number of quasars with $\phi \gtrsim 60°$. Given the assumptions stated in section 5.2, this implies a remarkably good alignment of the

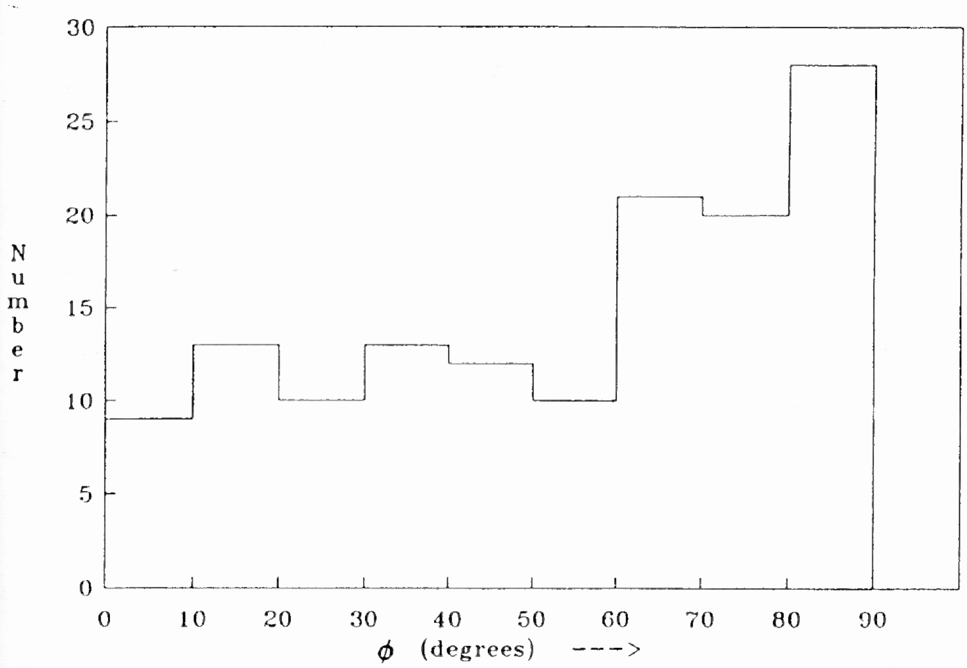

Fig.5.4 Distribution of the misalignment angle ϕ

nuclear jet with the radio axis. The axis of ejection of the radio emitting effluent must thus be stable for ~ 10^7 yr. On the other hand, the distribution also shows large misalignments for several other objects.

5.6 Are the misalignments intrinsic?

Are the above misalignments intrinsic and merely due to the presence of a bending/polarizing agent in those particular nuclei or their environs? This is indeed a possible interpretation. However, the findings of Readhead *et al.* (1983) naturally provoke one to investigate if whether this misalignment correlates with other structural properties, and whether these correlations go the way the unified scheme would predict.

5.6.1 The $\phi - R_{emit}$ correlation

The immediate correlation to look for is of course that of ϕ with R_{emit}. This is

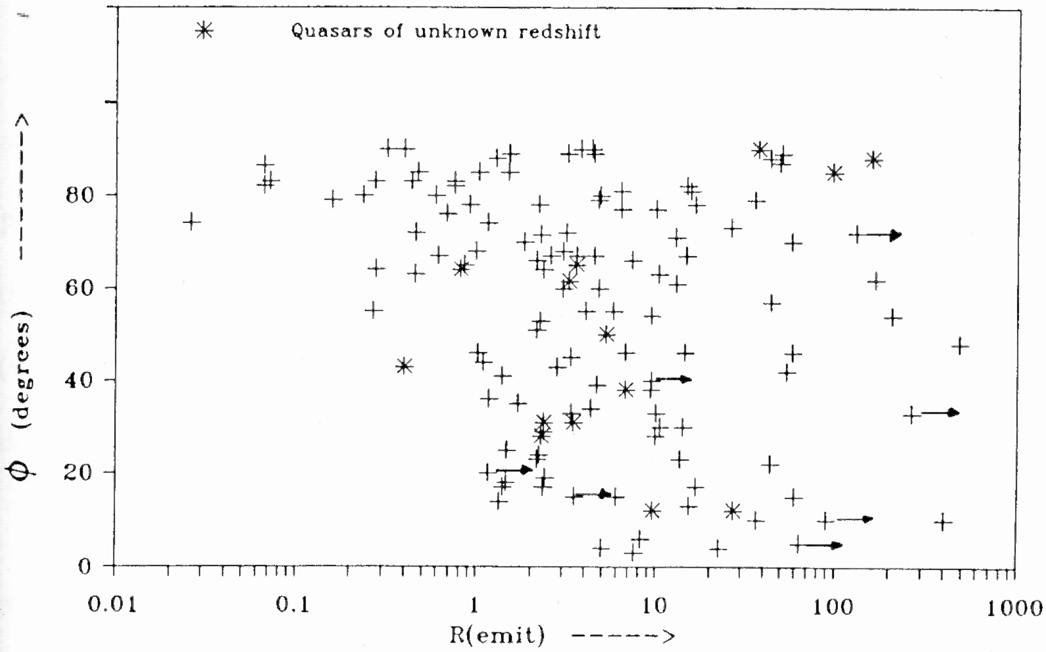

Fig. 5.5 Correlation of ϕ with R

plotted in Fig. 5.5 for the present sample of quasars. The diagram shows that ϕ ranges from ~ 10° to ~ 90° for quasars having R_{emit} >1, whereas for R_{emit} < 1, it is almost always between 60° and 90°. There is a distinct paucity of objects with low values of R_{emit} *and* large misalignments. Thus the qualitative trend seen here is indeed what the unified scheme would predict. The distributions of ϕ for the objects of the present sample bifurcated at $R_{emit} = 1$ are shown in Figs. 5.6a and b. Formally, a Kolmogorov-Smirnov two-tailed two-sample test indicates that the probability that the two subsamples are drawn from the same parent distribution is < 0.001.

5.6.2 Could it be just selection effects?

The sample of quasars under consideration is quite eclectic and far from being statistically complete; therefore the above correlation could, in principle, arise due to selection effects.

If the polarized flux density measurements for the objects with large R_{emit} had systematically lower values and therefore larger errors of measurement of the PA of polarization, then this would be reflected as a large scatter in their ϕ values. But the distributions of the degree of polarization for the quasars of the present sample (wherever available) with high and low values of R_{emit} (Figs. 5.7a and b) show that the degree of polarization is not systematically lower for the CDQs.

Could objects satisfying the selection criteria (i) and (ii) but not (iii) (i.e., those with misaligned outer lobes) fill up the paucity in Fig. 5.5? No, because as can be seen from Table 5.4 where these objects have been listed, they all have large values of R_{emit}, as indeed would be predicted by the unified scheme. Exclusion of these objects cannot therefore create a spurious paucity of sources with low R_{emit} *and*

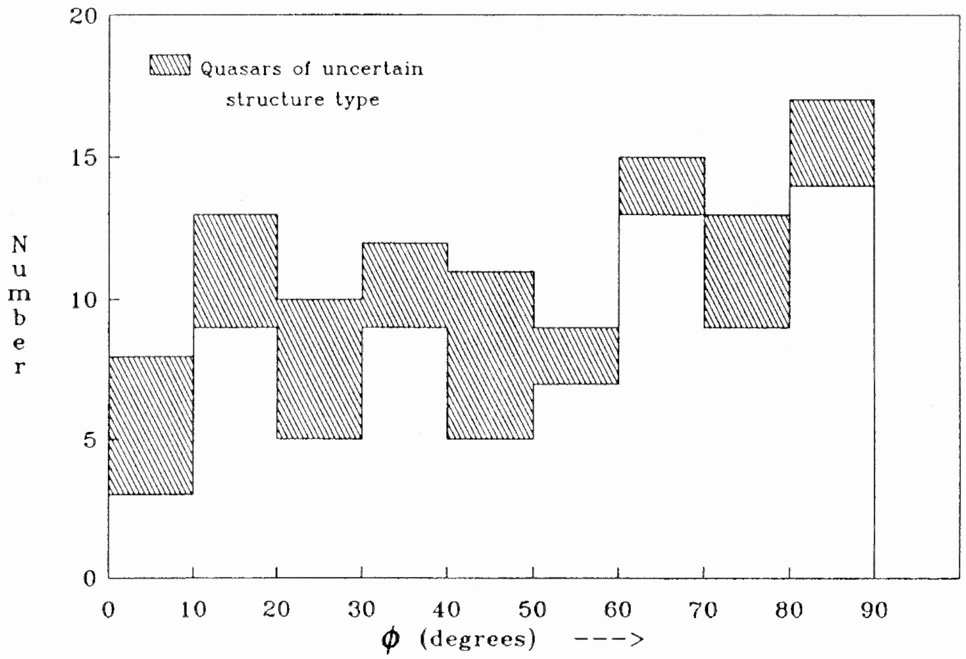

Fig. 5.6a Distribution of ϕ for quasars with R > 1

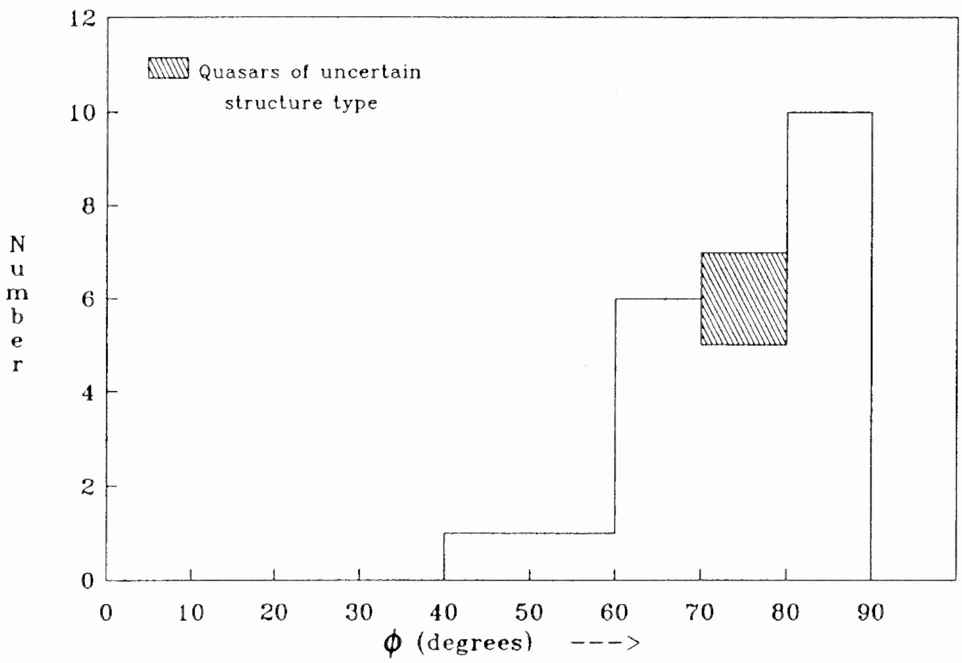

Fig. 5.6b Distribution of ϕ for quasars with R < 1

Fig. 5.7 Distribution of fractional polarization

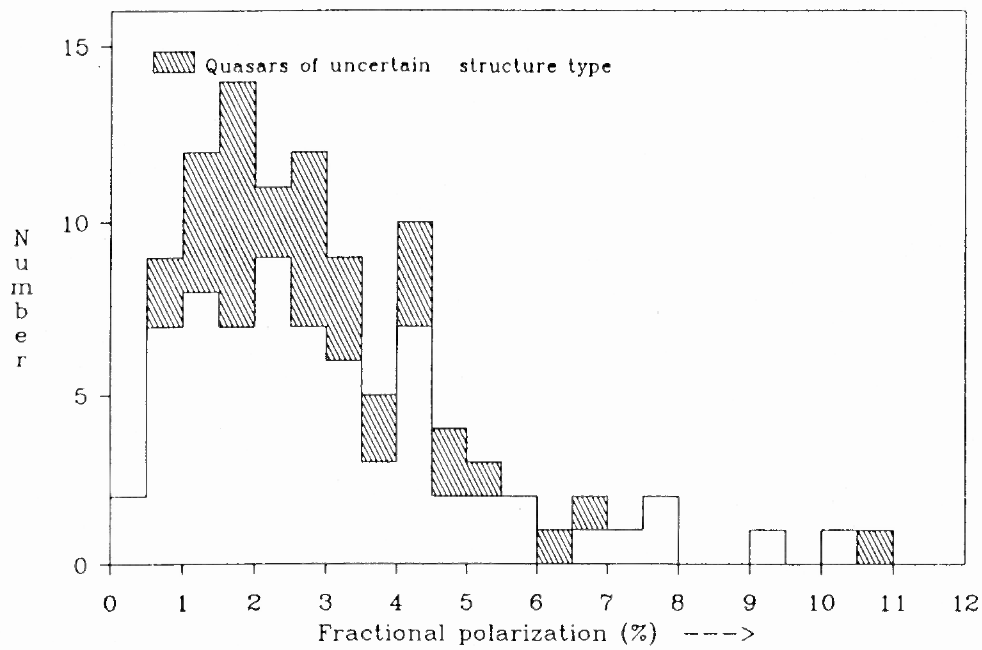

(a) Quasars with R > 1

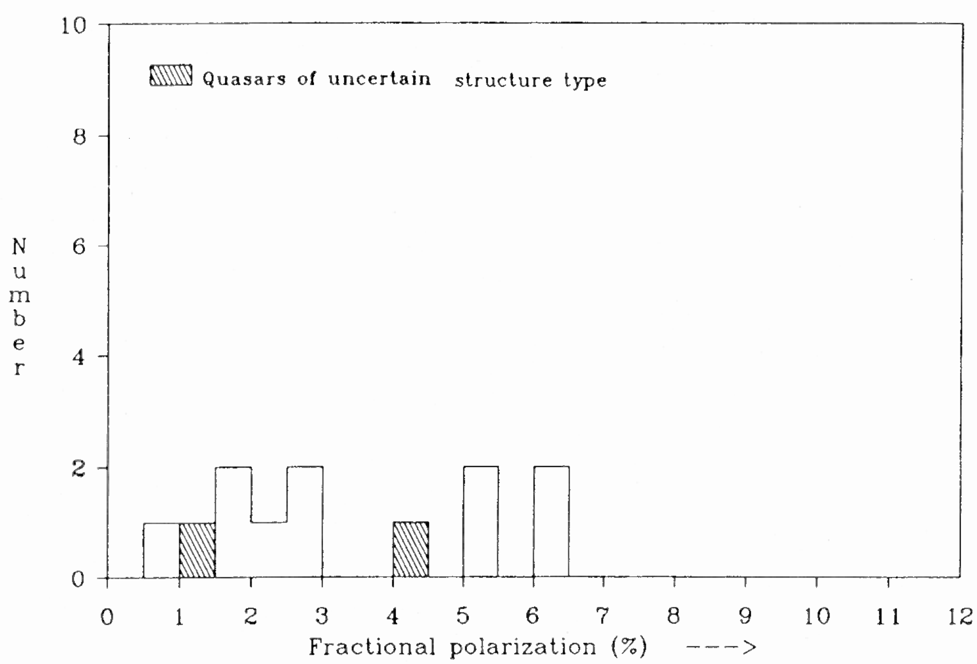

(b) Quasars with R < 1

Table 5.4 Quasars with highly misaligned outer lobes.

Source	Misalignment Angle (deg)	R	References
0119+041	49	> 4.7	P82;BP
0409+229	73	1.41	P82;present
0808+019	78	0.99	P82;AU
0814+425	85	> 8.0	P82;BP
0954+556	70	4.29	P82;B82a
1049+215	100	> 2.7	P82;BP
1253-055	57	2.54	P82;BP
1400+162	53	0.59	SSS
1641+399	53	282.78	P82;SdB
1823+568	75	7.45	P82;PFJ82
1924+507	54	6.44	OP
1928+738	35	11.06	P82;B87

large misalignments. It is hard to think of any other selection effect that would spuriously create a correlation of the kind presented in Fig. 5.5.

It must be pointed out that with better imaging, some of the quasars of uncertain radio structure in Perley (1982) might turn out to have large misalignments and would thereby have to be dropped from the sample by (criterion (iii)). But this would still not detract from the above correlation.

5.6.3 The connection with sidedness

Davis *et al.* (1978) found that, for the three 'one-sided' quasars they observed, the nuclei showed misalignments in marked contrast to 'two-sided' quasars. From this, they suggested that there may be a real connection between nuclear misalignment and the absence of a second outer component. Indeed there is. Fig. 5.8a and b present the distributions of ϕ for the quasars of the present sample bifurcated on the basis of sidedness. The objects with 'two-sided' structure clearly have a greater tendency to have nuclear and large scale structure aligned, while the

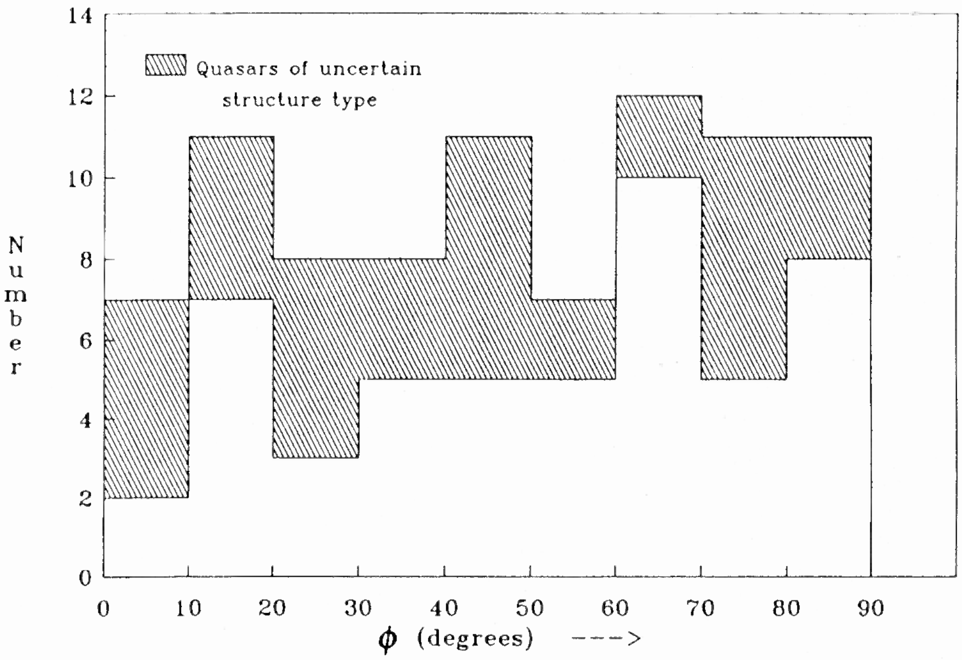

Fig. 5.8a Distribution of ϕ for one-sided quasars

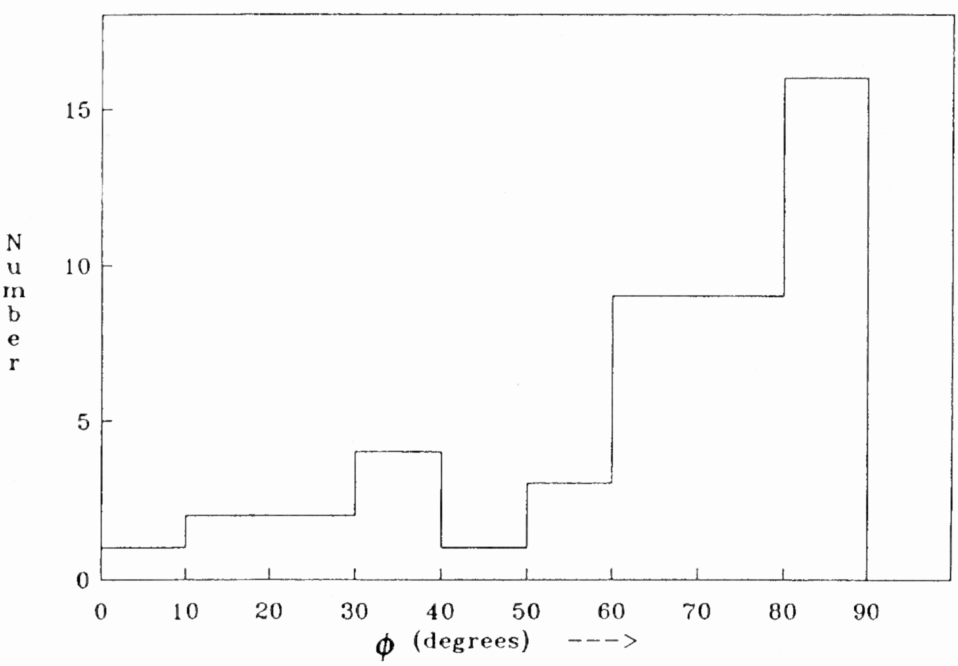

Fig. 5.8b Distribution of ϕ for two-sided quasars

Fig. 5.9 Distribution of fractional polarization

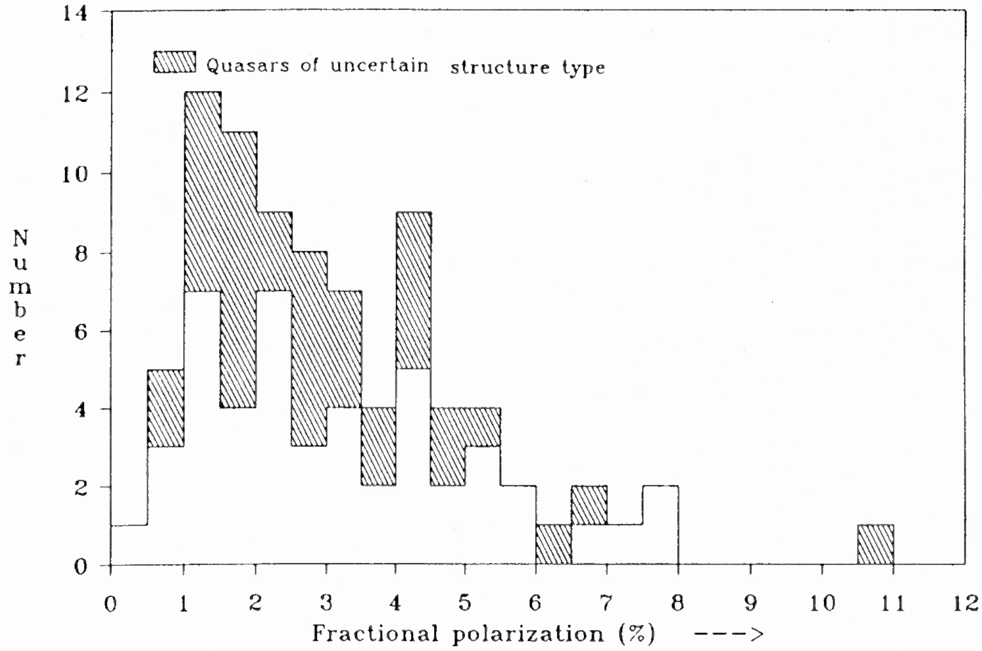

(a) One-sided quasars

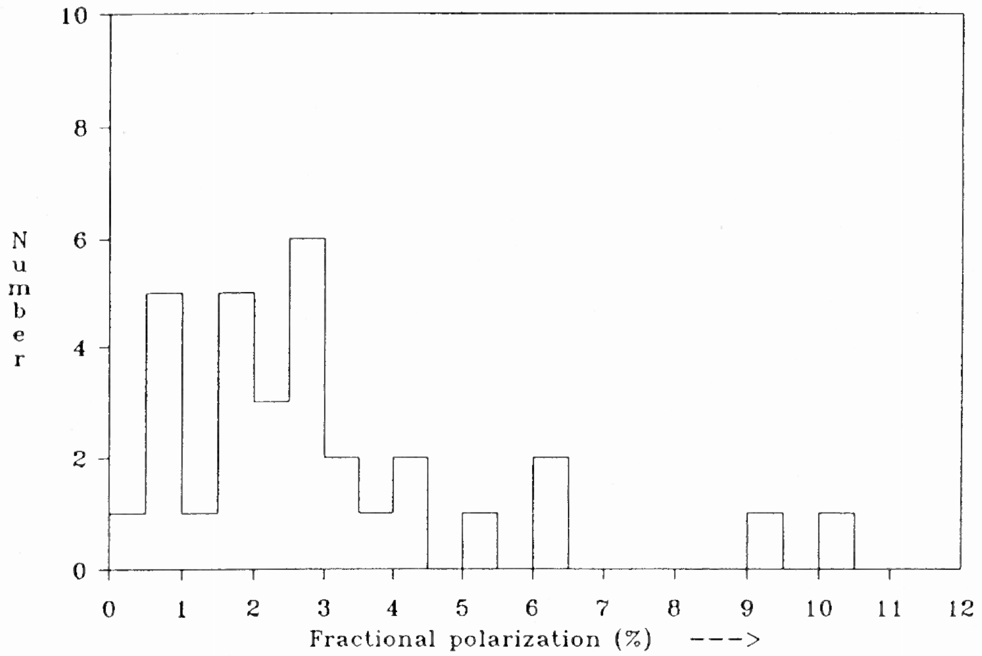

(b) Two-sided quasars

'one-sided' objects show large misalignments. A Kolmogorov-Smirnov two-tailed two-sample test shows that the probability that the two distributions are derived from the same parent distribution is <0.005. The trend is in accord with the interpretation of misalignment and of 'one-sidedness', viz., that 'one-sided' objects and misaligned objects are both sources oriented at small angles to the line of sight.

The distributions of the degree of polarization (whenever available) for the one- and two-sided objects are plotted in Figs 5.9a and b respectively. Once again it is clear that there is no systematic trend for the one-sided sources to have lower fractional polarization. This rules out the possibility that the nearly random distribution of ϕ for one-sided sources is due to larger errors in their PA of polarization.

It should be pointed out that the categorization of the sample into 'one-' and 'two-' sided sources is a very rough one, because the sample is eclectic and therefore the sensitivity and dynamic range of the radio images are not uniform; what appears as a 'one-sided' image with a certain dynamic range may well show structure on both sides of the nuclear component with finer imaging. However, the classification is not entirely meaningless, because it enables one to distinguish between objects of large and small surface brightness ratios of the outer components.

5.6.4 The $\phi - l$ relation

In Fig. 5.10, the projected linear size l, in kiloparsecs, is plotted against the misalignment parameter ϕ. l has been determined for a q_0 of 0.5 and H_0 of

50 km s^{-1} Mpc^{-1}. Projected linear sizes for those objects with no measured redshift were determined by assuming a redshift of 1, and these have been marked separately in the figure. It is clear from the $\phi - l$ relation that (for quasars with measured redshifts) almost all that have $l \gtrsim 200$ kpc have $\phi \gtrsim 60°$, while those with $l \lesssim 200$ kpc span the whole range of ϕ. This diagram is also consistent with the interpretation that quasars with a random distribution of ϕ are at small angles to the line of sight because they are then also expected to have smaller projected linear sizes due to foreshortening.

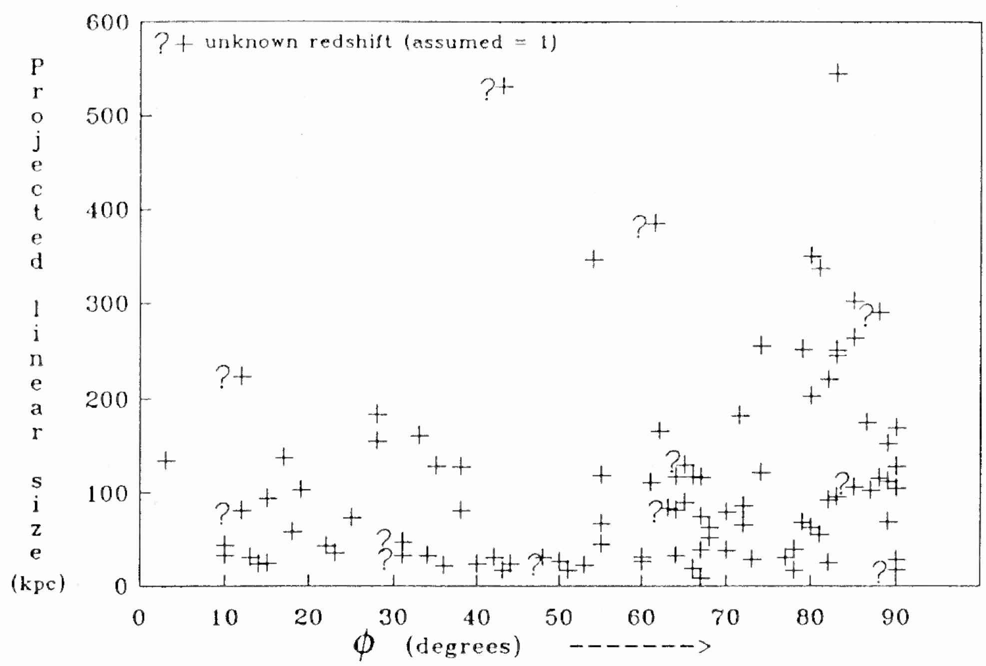

Fig.5.10 Projected linear size vs. ϕ

It should be noted that the quasars from Perley (1982) of uncertain structure-type have been excluded from this diagram. But this cannot create a spurious correlation of linear size with ϕ, because the quasars in question are, by their very selection, compact objects and of small projected linear sizes. Notably, even if their sizes (as given by Perley, 1982) are doubled to account for any missing outer component on the other side, they are still consistent with the $\phi - l$ correlation. There is one exception to the correlation, viz., 0742+376. This is a 'one-sided' source with a large projected linear size (as derived from an assumed redshift of 1). Its large size is however consistent with its low value of R_{emit}.

5.7 The case of radio sources identified with galaxies

A limited number of polarimetric measurements at high angular resolutions are available in the literature for radio galaxies also. It is therefore interesting to investigate whether the radio galaxies too follow any systematic trend. Antonucci (1984) has carried out such an investigation for eight radio galaxies and found that the polarization generally tends to be perpendicular to the radio structure axis. Galaxies that have available radio polarimetric measurements and properties of structure and sky position that meet the selection criteria listed in section 5.4 are tabulated in **Table 5.5** (a total of 17 sources). The objects from Antonucci (1984) are also included. The distribution of the parameter ϕ is shown in Fig. 5.11. The distribution shows that most of the objects have a value of $\phi \gtrsim 60°$. Taking the cue from the case of quasars, this trend probably reflects a similar physical phenomenon, *viz.*, that the magnetic field is parallel to the elongation of the nuclear radio jet in radio galaxies. Several measurements at slightly larger distances from the nucleus (e.g., Spangler & Pogge, 1984) also suggest this.

It must be pointed out here that no attempt has been made to distinguish between different kinds of galaxies, whether by optical type (for instance, elliptical, Seyfert, etc.) or by radio type (FR type I or II; Fanaroff & Riley, 1974). This could

Table 5.5 The sample of radio galaxies

Source	Alternate Name	core polarization PA (°)	Structure PA (°)	ϕ (°)	Reference
0111+021		47	120	73	Perley (1982)
0119+115		166	20	34	Perley (1982)
0206+135	4C35.03	14	132	62	Antonucci (1984)
0305+039		80	55	25	Perley (1982)
0338-214		123	90	33	Perley (1982)
0410+110	3C109	78	143	65	Antonucci (1984)
0430+052		166	136	30	Perley (1982)
0454+066		113	50	63	Perley (1982)
1128-047		60	116	56	Perley (1982)
1323-426	Cen A	69	132	63	Burns et al. (1983)
1330+022	3C287.1	171	90	81	Antonucci (1984)
1346+268	4C26.42	103	16	87	van Breugel et al.(1984)
1417-192		127	13	66	Antonucci (1984)
1441+522	3C303	5	116	69	Kronberg (1986)
1652+397	4C39.49	152	45	73	Antonucci (1984)
1807+698	3C371	162	60	78	Perley (1982)
2349-014	4C-01.61	58	170	68	Antonucci (1984)

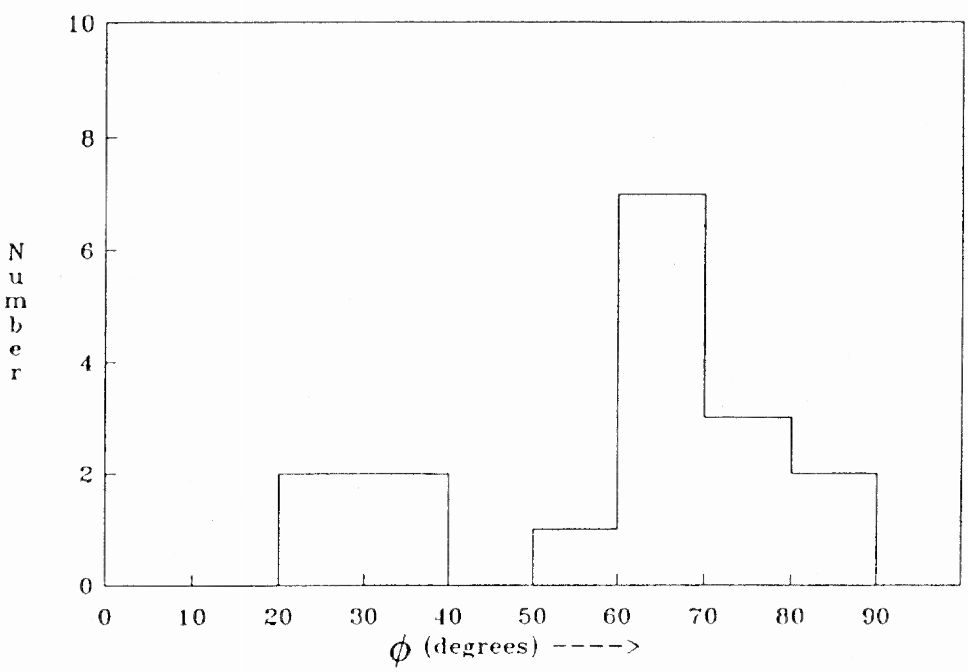

Fig. 5.11 Distribution of ϕ for radio galaxies

well be important, because the conditions in the nuclear regions would be different for different kinds of galaxies. Further, it would be illuminating to determine what role, if any, the nature of the optical emission line region plays in determining the nature of the observed polarized emission.

5.8 Are the RMs and depolarization dependent on orientation?

The results described in the earlier sections seem to suggest that the 'internal' RMs (due to Faraday rotation near the nuclear region) of the AGN under consideration are small. In view of the fact that sources with large R_{emit} show large misalignments of ϕ, it is important to investigate the dependence of the RM of the nuclear components on R_{emit} for quasars. Such a study is now under way. Polarimetric imaging with the VLA has been performed on a sample of radio quasars that were selected to have as large a range in R_{emit} values as possible from areas of sky with low Galactic RM (cf. Section 5.3).

Assuming that the unified scheme is valid, the above investigation is expected to lead to clues on the geometry of the Faraday rotating regions, and would thus also have a bearing on the results on quasar absorption lines that are now available. It has been suggested that the associated absorption at $z_{absorption} \approx z_{emission}$ in quasars occurs in absorbing clouds at distances of a few kiloparsecs from the QSO (Williams *et al.*, 1975). At resolutions $\lesssim$ 1 arcsec of the above polarimetric investigation, the physical regions sampled are of size similar to this at redshifts of ~ 1.5. Further, work by Foltz *et al.*(1987) on a sample of 88 radio-loud quasars has shown that strong associated absorption (within about ± 5000 km s^{-1} of the emission line redshift) was found in 22 of the objects, and there is a tendency for the absorption to occur preferentially in sources with steep radio spectrum. It would be interesting to examine if this dichotomy in the absorption characteristics is related to the observed Faraday rotation effects of the radio polarization.

5.9 Summary

The nuclear radio polarization of quasars has been used to infer the orientation of their nuclear jets. These jets appear well-aligned with the overall radio structure in the case of the LDQs, while CDQs often show large misalignments, consistent with the predictions of the unified scheme. Radio galaxies also appear to have their nuclear jets well-aligned with their radio axes. In view of the misalignments observed in CDQs, it is important to investigate if Faraday rotation in the nuclei of quasars is aspect dependent, and whether this might shed light on why associated absorption complexes appear to be preferentially in quasars of steep radio spectrum.